Metal–Organic Frameworks

DOI: 10.1002/anie.201108492

Transport into Metal–Organic Frameworks from Solution Is Not Purely Diffusive**

*Shuangbing Han, Thomas M. Hermans, Patrick E. Fuller, Yanhu Wei, and Bartosz A. Grzybowski**

In virtually all applications of metal–organic frameworks (MOFs),[1] it is important to understand and quantify the transport through their nanoscopic channels.[2] To date, most studies have focused on gas-phase systems and their modeling using molecular dynamics (MD) simulations. This effort has provided a wealth of information on the self-, corrected, and transport diffusivities of molecules from the gas phase into the MOF bulk.[3,4] Significantly fewer studies have examined molecular transport into solvent-filled MOFs[1b,5] which is becoming increasingly important in heterogeneous catalysis. In the vast majority of these works, the transport has been described as simple Fickian diffusion.[5a,6] Here, we combine experiment with theory to show that such a pure diffusion approach is a gross oversimplification and, instead, transport equations should be of the reaction-diffusion (RD) form. The RD description is appropriate at both the macroscopic scale (studied using the dye diffusion profiles) and the nanoscale (studied using fluorescence correlation spectroscopy).

Currently available techniques for the quantification of transport into nano- or microporous materials (e.g., zeolites,[7] MOFs) include quasi-elastic neutron scattering (QENS),[8] pulsed field gradient nuclear magnetic resonance (PFG NMR),[9] interference microscopy (IFM) and infrared microscopy (IRM).[6a–b,10] In particular, IFM and IRM, recently developed by Kärger's group, are two techniques which can monitor diffusion in individual nanoporous crystallites, though they cannot easily extract full, three-dimensional concentration profiles[11]—this difficulty might explain why both techniques have not yet been widely used. Other techniques, such as luminescence quenching[5a] and quartz-crystal microbalance (QCM),[6c] provide diffusivity data that are averaged over one or more MOF particles. As mentioned above, the concentration profiles observed during infusion of the MOF are usually explained using pure or effective diffusion models. While in some cases this approach seems to fit the data reasonably well,[5a,6] there are other instances where it does not—for example, in the separations of liquid mixtures over MOF-crystal "columns" we recently described.[1b]

The motivation for the present work is therefore two-fold. First, we wish to develop an experimental method in which the diffusion profiles into MOFs could be studied directly and without ambiguity and, importantly, using equipment that is available to most research groups. Second, we wish to provide a general theoretical framework with which to study transport into MOFs from solution. To meet these objectives, we combine the ability to grow large, millimeter-sized MOF crystals[1b,12] (here, MOF-5) with confocal laser scanning microscopy (CLSM)[13] and fluorescence correlation spectroscopy (FCS)[14] which have been previously applied to measure the transport of dyes or fluorescently labeled molecules into protein crystal and other materials. The concentration profiles we reconstruct using these techniques rule out the popular—but as it turns out, incorrect—pure diffusion description of the transport process and instead suggest that a reaction-diffusion process[15] is operative, in which sorption of the analyte is markedly enhanced by favorable interactions between the diffusing molecules and the MOF scaffold.[16]

Millimeter-sized (from around $0.3\times0.3\times0.15$ to $2\times2\times1\ mm^3$) single MOF-5[17] crystals (Figure 1) were prepared from $Zn(NO_3)_2\cdot6H_2O$ and terephthalic acid in diethylformamide (DEF) using a solvothermal procedure as described in our previous papers.[1b,12] These crystals comprise nanometer-sized cavities and intercrossing 1D channels (cross-section around $8\times8\ Å^2$) running along perpendicular directions (Figure 1a). The crystals were stored in dimethylformamide (DMF) and immersed in a DMF solution of pyronin B (PB) during CSLM imaging. DMF was chosen as solvent because it does not compromise the structural integrity of the MOF scaffold during dye diffusion[1b] (see also the Supporting Information, section 2 for crystallographic studies of the MOF and the MOF soaked with PB). PB was chosen as a diffusing "guest" because of its high quantum yield[18] which allowed for the use of very low concentrations (≤ 100 nM) at which fluorescence intensity is linearly proportional to the concentration of PB (see the Supporting Information, section 1). Moreover, the optical density was low enough to allow the laser light to fully penetrate the entire MOF-5 crystal and minimize reabsorption. The submerged crystals were placed onto a furfuryl amido-bisphenol A diglycidyl

[*] Dr. S. Han,[+] Dr. Ir. T. M. Hermans,[+] P. E. Fuller, Dr. Y. Wei, Prof. Dr. B. A. Grzybowski
Department of Chemical and Biological Engineering
Department of Chemistry, Northwestern University
2145 Sheridan Road, Evanston, IL 60208 (USA)
E-mail: grzybor@northwestern.edu
Homepage: http://dysa.northwestern.edu

[+] These authors contributed equally to this work.

[**] This work was supported by the Non-equilibrium Energy Research Center which is an Energy Frontier Research Center funded by the U.S. Department of Energy, Office of Science, Office of Basic Energy Sciences under grant number DE-SC0000989. T.M.H. is funded by the Human Frontier Science Program. We thank Prof. Dr. G. Fytas (University of Crete, IESL-FORTH and Max Planck Institute for Polymer Research Mainz) for helpful suggestions on the interpretation of the fluorescence correlation spectroscopy results.

Supporting information for this article is available on the WWW under http://dx.doi.org/10.1002/anie.201108492.

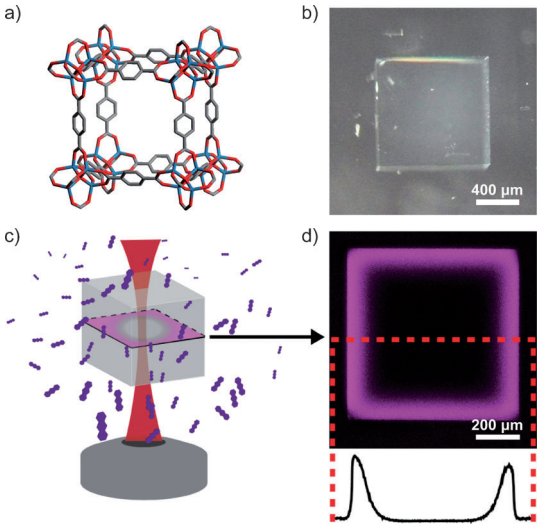

Figure 1. a) A cubic unit cell of a MOF-5 crystal. b) An optical micrograph of a millimeter-sized MOF-5 crystal. c) Experimental setup, in which a single MOF-5 crystal is immersed in a solution of a fluorescent dye (pyronin B) and the three-dimensional intensity/concentration profile is reconstructed using confocal laser scanning microscopy. d) A typical confocal image of an *xy* section inside of the crystal illustrating the diffusion of the dye (purple). The curve below shows the fluorescence intensity along the horizontal dashed line.

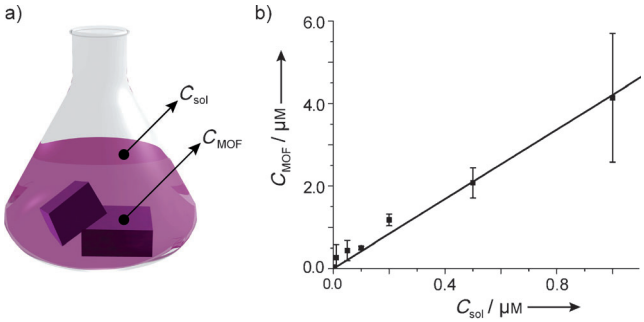

Figure 2. a) Schematic illustration of MOF-5 crystals in a PB solution (not to scale). The equilibrium PB concentration inside MOF-5 crystals (C_{MOF}) and the PB solution concentration (C_{sol}) are indicated. b) C_{MOF} versus C_{sol} measured by fluorimetry (see the Experimental Section), which clearly shows that the PB concentration inside the MOF-5 is higher than in solution. Error bars correspond to standard deviations from three independent experiments.

ether (FA-BADE) organogel (see ref. [1b,12] for synthetic details) to ensure equal influxes of PB from all crystal faces (note: when the crystals were placed directly at the bottom of a glass dish, the influx through the bottom crystal plane was significantly lower). Three-dimensional (*xyz*) concentration profiles of PB within the MOF crystals (Figure 1c,d) were acquired on a Nikon A1R confocal microscope with XY slices (512 × 512 pixels, 2.49 μm per pixel, four line averages) taken every 10 μm and reconstructed into three-dimensional volumes using Bitplane Imaris 7.3.0 software. During imaging, the laser power was set as low as possible (10–20%, 1 mW HeNe laser) to avoid fluorescence saturation and to minimize photobleaching. To obtain time-dependent PB concentration profiles in the MOF, images were acquired at 3 to 10 min intervals (for time evolution of these profiles, see the Supporting Information, Movie 1).

To study the transport into the MOFs quantitatively, it is necessary to ascertain that the measured fluorescence intensity is proportional to the concentration of dye inside the MOF crystals. To do so, we first generated a calibration curve by measuring the fluorescence emission intensities at 620 nm (excited at 500 nm) of a series of PB solutions of concentrations ranging from 1 nM to 1 μM (see Figure S1 in the Supporting Information, section 1,). Next, we prepared a series of dye-equilibrated crystals by immersing MOF-5 crystals in 1 nM to 1 μM PB for 4–5 days (Figure 2a). The equilibrium concentrations of PB in the MOF-5 were determined by completely dissolving the soaked crystals, measuring the fluorescence of the solutions thus obtained and comparing with the calibration curve. The key finding of this study was that over the concentration range we examined, the equilibrium concentration of PB inside the MOF was (5.59 ± 1.9)-times higher than the concentration of PB in the solutions in which the MOFs were soaked (Figure 2b). This result shows clearly that transport of the dye into the MOF cannot be purely diffusive—if it were, concentration in the crystals should not exceed the solution concentration. Instead, the MOF "concentrates" the dye from solution by virtue of the energetically favorable interactions between the dye molecules and the MOF scaffold.[1b] In terms of quantitative description, accounting for such interactions requires the use of reaction-diffusion equations which for our system can be written as Equation (1):[15]

$$\begin{aligned} \partial[\mathrm{PB}]/dt &= D_{\mathrm{PB}}\nabla^2[\mathrm{PB}] - R \\ \partial[\mathrm{S^*}]/dt &= -R \\ \partial[\mathrm{PB\cdot S}]/dt &= R \end{aligned} \qquad (1)$$

where [PB] stands for the concentration of diffusing PB (linearly proportional to the fluorescence signal, see Figure S2 in the Supporting Information), [S*] is the concentration of unoccupied sites on the MOF scaffold with which PB can interact, and [PB·S] is the concentration of occupied sites. All of these quantities depend both on time and on the position within the MOF. The reaction term reflects the chemical equilibrium established between the bound and unbound PB molecules, and can be written as $R = k_1[\mathrm{PB}][\mathrm{S^*}] - k_{-1}[\mathrm{PB\cdot S}]$, where k_1 and k_{-1} are the association and dissociation rate constants, respectively. Since the characteristic timescale for the PB/MOF interaction is much shorter than the diffusion timescale[15a,c,19] (also verified by FCS measurements described below), their ratio $K_{eq} = k_1/k_{-1}$ can be determined reliably as reported in other reaction-diffusion systems.[15c,20]

The RD equations were solved numerically using the Crank–Nicolson algorithm[15d,21] with the initial conditions (time $t = 0$) inside the MOF given by $[\mathrm{PB}]_0 = 0$ M, $[\mathrm{S^*}]_0 = 0.79$ M,[22] and $[\mathrm{PB\cdot S}]_0 = 0$ M, and the boundary condition setting the PB concentration outside of the MOF crystal as constant, $[\mathrm{PB}] = 10^{-7}$ M (since the number of molecules in solution is thousands of times higher than the maximum

number of PB molecules adsorbed into the crystal). The RD equations were solved for different trial values of the D_{PB} and K_{eq} parameters, the optimal values of which were then found by minimizing the quadratic error between the experimental and modeled concentration profiles; this procedure was performed according to the Nelder–Mead simplex algorithm.[15]

Examples of experimental versus modeled concentration profiles are shown in Figure 3. The best fit to the experimental

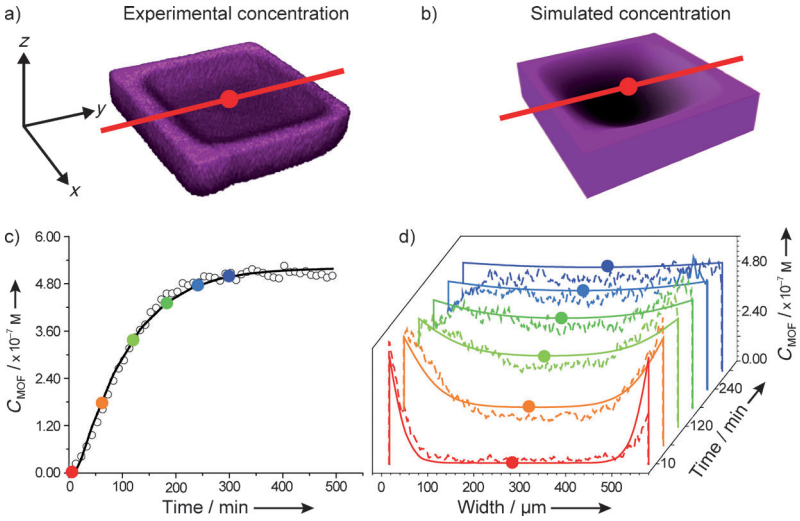

Figure 3. a) A typical 3D experimental concentration profile of PB migrating into a single MOF-5 crystal (here, 729×749×250 µm, image taken at t = 46 min) reconstructed using CSLM. Only the bottom half of the 3D concentration profile is shown for clarity. The red dot in the middle indicates the center of the crystal. b) The corresponding simulated 3D concentration profile. c) The measured concentration of PB at the exact center of the MOF-5 crystal (circles)—that is, measured by CLSM at the location marked with the red dot in (a,b). The solid line is the theoretical dependence predicted by the reaction-diffusion model described in the main text. The colored points correspond to the times shown in (d). d) An overlay of experimental PB concentration profiles (dashed) and corresponding RD fits (solid) along the middle of the crystal (i.e., along the solid red line in (a,b) at different times)

data is achieved for the diffusion coefficient of $(6.81 \pm 2.10) \times 10^{-12}$ m^{2}s^{-1} and an equilibrium binding constant K_{eq} of (6.72 ± 0.41) M^{-1}. We note that the fitted value of K_{eq} agrees with that estimated from the titration experiments. This can be shown by considering the fractional occupancy of the MOF sites $\theta = [PB{\cdot}S]/([PB{\cdot}S] + [S^*])$ and rearranging the definition of the equilibrium constant into the form of a familiar Langmuir isotherm, $K_{eq}[PB] = \theta/(1-\theta)$. For the very dilute concentrations we use, this simplifies to Henry's law: $K_{eq}[PB] = \theta$. As at equilibrium the concentration of the unbound dye is equal to its solution concentration, and estimating θ from the titration data in Figure 2b yields $K_{eq} = (4.06 \pm 0.37)$ M^{-1}, which is indeed close to the value obtained using our reaction-diffusion model.

Having established reaction-diffusion transport into the MOF, we further studied the nanoscale aspects of this process using FCS, which measures temporal changes in emitted fluorescence intensity by few molecules (< 10) in a very small (fL) sample volume, the so-called confocal volume (Figure 4a).[23]

As PB molecules move in and out of the confocal volume within the MOF, they cause the measured fluorescence intensity to fluctuate. The intensity fluctuations can be time-correlated using the autocorrelation function $G(\tau)$ of Equation (2):

$$G(\tau) = \frac{\langle I(t)I(t+\tau)\rangle}{\langle I(t)\rangle^2} \qquad (2)$$

which gives the correlation coefficient between the fluorescence intensity at time t, $I(t)$, with the intensity at a later time, $I(t+\tau)$. For a freely diffusing fluorescent molecule this autocorrelation function can be analyzed using a diffusion model [Eq. (3)]:[24]

$$G_D(\tau) = 1 + \frac{1}{N}\left(1 + \frac{\tau}{\tau_D}\right)^{-1}\left(1 + \frac{\tau}{w^2\tau_D}\right)^{-1/2} \qquad (3)$$

where N is the number of particles in the confocal volume, w is the structure parameter ($w = w_z/w_{xy} = 11.5$, see Figure 4a) and τ_D is the diffusion time, which is directly related to the respective diffusion coefficient D $\left(D = w_{xy}^2/4\tau_D\right)$.

In the context of our experiments, we first used the equation for $G_D(\tau)$ to model the "free" diffusion of PB in 10 nM solution of DMF. This analysis (Figure 4b, black circles), gave the value of $\tau_D = (53.6 \pm 11.1)$ µs, corresponding to a diffusion coefficient of $(3.26 \pm 0.56) \times 10^{-10}$ m^{2}s^{-1}, in close agreement with its literature value.[24]

A completely different correlation curve was observed for PB moving inside the MOF, where the typical time lag (τ) is three orders of magnitude larger (Figure 4b, red squares) than

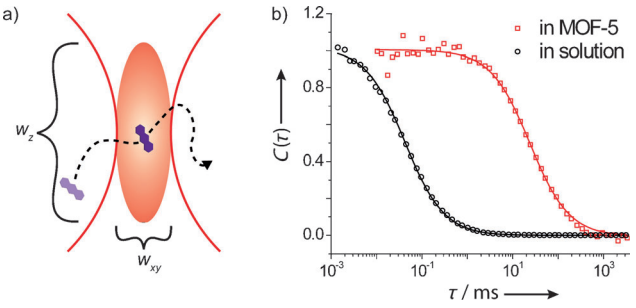

Figure 4. a) Fluorescence correlation spectroscopy measures and correlates fluctuations in fluorescence intensity within the confocal volume (i.e., the oblate ellipsoid with width w_{xy} and height w_z). Here, fluorescence intensity fluctuations are due to the diffusion of PB molecules in and out of the confocal volume. b) Normalized correlation function $C(\tau)$ (i.e., $G(\tau)$ normalized from 0 to 1) versus time lag, τ. The black circles are for the diffusion of 10 nM PB in DMF solution—this dependence is analyzed using the $G_D(\tau)$ function [Eq. (3)]. The red squares are for the migration of PB inside the MOF crystal and are analyzed using $G_{RD}(\tau)$ [Eq. (4)]. The solid lines are fits described in the main text.

for the free diffusion case. As described above for the confocal imaging studies, this difference is due to the fact that not only diffusion but also the interaction of PB with the MOF scaffold has to be taken into account. Therefore, the experimentally measured correlation function $G(\tau)$ needs to be analyzed using a reaction-diffusion model [Eq. (4)],[24]

$$G_{RD}(\tau) = 1 + \frac{1}{N_G + N_{GS}}\left(1+\frac{\tau}{\overline{\tau_D}}\right)^{-1}\left(1+\frac{\tau}{w\overline{\tau_D}}\right)^{-1/2}[1 + A\exp(-\tau/\tau_R)]$$
$$\tau_R = (k_1[S^*] + k_{-1}),\ \text{for } [S^*] \gg [PB],\ \text{thus } [S^*] = [S^*]_0 \quad (4)$$

where N_G and N_{GS} are the number of unbound and bound PB molecules, $\overline{\tau_D}$ is the mean diffusion time of PB molecules between their bound and unbound states, w is the structure factor, τ_R is the reaction time (i.e., $1/R$ described above, assuming pseudo-first order) and A is the reaction amplitude, which corrects for differences in fluorescence brightness of PB in bound and unbound states.[24]

The reaction-diffusion model $G_{RD}(\tau)$ gives $\overline{\tau_D} = (47 \pm 22)$ ms which translates into a mean diffusion coefficient $\overline{D_{FCS}} = (5.31 \pm 0.17) \times 10^{-13}\ m^2 s^{-1}$. This value is in general agreement with the mean diffusion coefficient that can be derived from the CLSM/RD studies—specifically, using the values of $K_{eq} = (6.72 \pm 0.41)\ M^{-1}$ and $D_{PB} = (6.81 \pm 2.10) \times 10^{-12}\ m^2 s^{-1}$, the CLSM data can be used to calculate the mean diffusion coefficient $\overline{D_{CLSM}} = (1-\theta_{PB})D_{PB} = (1.03 \pm 0.32) \times 10^{-12}\ m^2 s^{-1}$, where θ_{PB} is the molar fraction of bound PB molecules (see the Experimental Section). The agreement between $\overline{D_{FCS}}$ and $\overline{D_{CLSM}}$, indicates that the transport behavior of PB in MOF-5 is governed by the same reaction-diffusion mechanism on all the length scales analyzed (i.e., from nanometers to hundreds of micrometers). It should be emphasized, however, that the use of the CLSM/RD and FCS techniques is not redundant but rather complimentary, as each of the methods has its limitations. CLSM/RD is appropriate to study only the macroscale manifestations of RD; the FCS approach is relatively insensitive to the values of A and τ_R (see FCS in the Experimental Section) indicating that this method alone cannot directly determine k_1 and k_{-1} (and thus K_{eq}) parameters.

In conclusion, we used various modalities of confocal microscopy to quantify molecular transport from solution into macroscopically sized MOF single crystals. The main finding of this work is that simple and often used pure diffusion models are insufficient to describe this process and, instead, it is crucially important to account for the interactions of the guest molecules with the MOF scaffold.

Experimental Section

Imaging of the dye concentration profiles using confocal laser scanning microscopy: The PB diffusion and the evolution of concentration profiles in the whole crystal were recorded using confocal laser scanning microscopy (on a Nikon A1 system) within around 3 min after MOF-5 crystals were immersed in a 100 nM solution of pyronin B in DMF. The standard Cy5 filter sets were used exciting the dye at 543.5 nm. Multiple MOF crystals were imaged sequentially by using a motorized stage. Z-stacks typically comprised 20 to 50 images (at 10 μm intervals) recorded using a 10X plan air objective at 1 airy unit (i.e. optical slice of 0.85 μm). Glass-bottom Petri-dishes were obtained from VWR.

Fluorescence correlation spectroscopy: A Zeiss 510 Meta confocal microscope equipped with the Confocor3 module combined with a 40X water objective was used. At least 5×10^6 photon counts were collected at a count rate of 50–100 kHz. All measurements were performed at room temperature (22 °C). The photon counter module detects any changes in signal intensity, which are caused by various fast photophysical phenomena, such as triplet-state decay and blinking, and slower phenomena such as translational diffusion. For simplicity the contribution of triplet state decay is omitted from the diffusion equation in the main text.

Measurements of 10 seconds were collected and discarded if they had a triplet fraction (T_t) higher than 0.25 or a characteristic triplet time (τ_t) higher than 10 ms. The setup was calibrated using a 10 nM aqueous solution of Rhodamine B with a known diffusion coefficient of $(2.9 \pm 0.7)\ m^2 s^{-1}$, which was used to calculate the structure factor w (11.5) under Gaussian illumination.

For $K_{eq} = (6.72 \pm 0.41)\ M^{-1}$, the fraction of bound PB molecules during the FCS experiments (at PB concentration of 10 nM) is 0.85 ± 0.01. The observed mean diffusion coefficient determined by CLSM is given in Equation (5),

$$\overline{D_{PB}} = (1-\theta_{PB})D_{PB,unbound} + \theta_{PB}\, D_{PB,bound} \quad (5)$$

where $D_{PB,unbound}$ is the diffusion coefficient of unbound PB molecules and $D_{PB,bound}$ is the diffusion coefficient of bound PB molecules ($=0$). Therefore, only the first term is stated in the main text and $D_{PB,unbound}$ is written and D_{PB}.

A Levenberg–Marquardt algorithm was used to fit the reaction-diffusion model $G_{RD}(\tau)$, but was insensitive toward A and τ_R. This was also observed in a study by Al-Soufi et al.:[24] τ_R is found in the regime dominated by triplet state decay and antibunching processes ($< 10^{-3}$ ms) making it very hard for it to be determined.

Concentration of PB in MOF-5 crystals by fluorimetry: Fluorescence excitation and emission spectra and single point emission intensity of PB solutions were recorded using an ISS PC1 photon counting fluorimeter. For single point emission measurements, the excitation wavelength was 500 nm and the emission wavelengths 600 and 620 nm, respectively.

Received: December 2, 2011
Published online: February 1, 2012

Keywords: confocal laser scanning microscopy · fluorescence spectroscopy · metal–organic frameworks · reaction-diffusion models

[1] a) J. R. Li, R. J. Kuppler, H. Zhou, *Chem. Soc. Rev.* **2009**, *38*, 1477–1504; b) S. Han, Y. Wei, C. Valente, I. Lagzi, J. J. Gassensmith, A. Coskun, J. F. Stoddart, B. A. Grzybowski, *J. Am. Chem. Soc.* **2010**, *132*, 16358–16361; c) L. Ma, J. M. Falkowski, C. Abney, W. Lin, *Nat. Chem.* **2010**, *2*, 838–846; d) D. Farrusseng, S. Aguado, C. Pinel, *Angew. Chem.* **2009**, *121*, 7638–7649; *Angew. Chem. Int. Ed.* **2009**, *48*, 7502–7513.

[2] C. Chmelik, J. Kärger, *Chem. Soc. Rev.* **2010**, *39*, 4864–4884.

[3] a) L. Sarkisov, T. Düren, R. Q. Snurr, *Mol. Phys.* **2004**, *102*, 211–221; b) A. I. Skoulidas, D. S. Sholl, *J. Phys. Chem. B* **2005**, *109*, 15760–15768; c) R. Babarao, Y. H. Tong, J. W. Jiang, *J. Phys. Chem. B* **2009**, *113*, 9129–9136.

[4] F. Salles, H. Jobic, A. Ghoufi, P. L. Llewellyn, C. Serre, S. Bourrelly, G. Férey, G. Maurin, *Angew. Chem.* **2009**, *121*, 8485–8489; *Angew. Chem. Int. Ed.* **2009**, *48*, 8335–8339.

[5] a) C. Wang, W. Lin, *J. Am. Chem. Soc.* **2011**, *133*, 4232 – 4235; b) H. J. Choi, M. P. Suh, *J. Am. Chem. Soc.* **2004**, *126*, 15844 – 15851.

[6] a) C. Chmelik, J. Kärger, *Adsorption* **2010**, *16* 515 – 523; b) P. V. Kortunov, L. Heinke, M. Arnold, Y. Nedellec, D. J. Jones, J. Caro, J. Kärger, *J. Am. Chem. Soc.* **2007**, *129*, 8041 – 8047; c) O. Zybaylo, O. Shekhah, H. Wang, M. Tafipolsky, R. Schmid, D. Johannsmann, C. Wöll, *Phys. Chem. Chem. Phys.* **2010**, *12*, 8092 – 8097.

[7] a) H. G. Karge, J. Kärger, *Adsorption and Diffusion. Molecular Sieves, Vol. 7*, Springer, Berlin, **2008**, pp. 135 – 206; b) H. Jobic, D. N. Theodorou, *Microporous Mesoporous Mater.* **2007**, *102*, 21 – 50.

[8] a) F. Salles, H. Jobic, T. Devic, P. L. Llewellyn, C. Serre, G. Férey, G. Maurin, *ACS Nano* **2010**, *4*, 143 – 152; b) N. Rosenbach, Jr., H. Jobic, A. Ghoufi, F. Salles, G. Maurin, S. Bourrelly, P. L. Llewellyn, T. Devic, C. Serre, G. Férey, *Angew. Chem.* **2008**, *120*, 6713 – 6717; *Angew. Chem. Int. Ed.* **2008**, *47*, 6611 – 6615.

[9] a) F. Stallmach, S. Gröger, V. Künzel, J. Körger, O. M. Yaghi, M. Hesse, U. Müller, *Angew. Chem.* **2006**, *118*, 2177 – 2181; *Angew. Chem. Int. Ed.* **2006**, *45*, 2123 – 2126; b) M. Wehring, J. Gascon, D. Dubbeldam, F. Kapteijn, R. Q. Snurr, F. Stallmach, *J. Phys. Chem. C* **2010**, *114*, 10527 – 10534; c) J. Kärger, J. Caro, P. Cool, M.-O. Coppens, D. Jones, F. Kapteijn, F. Rodríguez-Reinoso, M. Stöcker, D. Theodorou, E. F. Vansant, J. Weitkamp, *Chem. Eng. Technol.* **2009**, *32*, 1494 – 1511; d) R. Valiullin, J. Kärger, R. Gläser, *Phys. Chem. Chem. Phys.* **2009**, *11*, 2833 – 2835.

[10] a) C. Chmelik, L. Heinke, R. Valiullin, J. Kärger, *Chem. Ing. Tech.* **2010**, *82*, 779 – 804; b) C. Chmelik, L. Heinke, P. Kortunov, J. Li, D. Olson, D. Tzoulaki, J. Weitkamp, J. Käger, *ChemPhysChem* **2009**, *10*, 2623 – 2627.

[11] a) L. Heinke, P. Kortunov, D. Tzoulaki, M. Castro, P. A. Wrightand, J. Kärger, *Europhys. Lett.* **2008**, *81*, 26002; b) D. Tzoulaki, L. Heinke, M. Castro, P. Cubillas, M. W. Anderson, W. Zhou, P. Wright, J. Kärger, *J. Am. Chem. Soc.* **2010**, *132*, 11665 – 11670.

[12] S. Han, Y. Wei, C. Valente, R. S. Forgan, J. J. Gassensmith, R. A. Smaldone, H. Nakanishi, A. Coskun, J. F. Stoddart, B. A. Grzybowski, *Angew. Chem.* **2011**, *123*, 290 – 293; *Angew. Chem. Int. Ed.* **2011**, *50*, 276 – 279.

[13] a) A. Cvetkovic, A. J. J. Straathof, D. N. Hanlon, S. van der Zwaag, R. Krishna, L. A. M. van der Wielen, *Biotechnol. Bioeng.* **2004**, *86*, 389 – 398; b) M. D. Burke, J. O. Park, M. Srinivasarao, S. A. Khan, *Macromolecules* **2000**, *33*, 7500 – 7507; c) R. Archipov, A. Cvetkovic, F. Stallmach,, A. J. J. Straathof, *Microporous Mesoporous Mater.* **2008**, *112*, 474 – 480.

[14] J. A. J. Fitzpatrick, B. F. Lillemeier, *Curr. Opin. Struct. Biol.* **2011**, *21*, 650 – 660.

[15] a) B. A. Grzybowski *Chemistry in Motion: Reaction-Diffusion Systhems for Micro- and Nanotechnology*; Wiley, New York, **2009**, chap. 4, pp. 61 – 91; b) P. J. Wesson, S. Soh, R. Klajn, K. J. M. Bishop, T. P. Gray, B. A. Grzybowski, *Adv. Mater.* **2009**, *21*, 1911 – 1915; c) Y. Wei, P. J. Wesson, I. Kourkine, B. A. Grzybowski, *Anal. Chem.* **2010**, *82*, 8780 – 8784; d) S. Soh, M. Byrska, K. Kandere-Grzybowska, B. A. Grzybowski, *Angew. Chem.* **2010**, *122*, 4264 – 4294; *Angew. Chem. Int. Ed.* **2010**, *49*, 4170 – 4198; e) Y. Wei, S. Soh, M. M. Apodaca, J. Kim, B. A. Grzybowski, *Small* **2010**, *6*, 857 – 863; f) B. A. Grzybowski, K. J. M. Bishop, C. J. Campbell, M. Fialkowski, S. K. Smoukov, *Soft Matter* **2005**, *1*, 114 – 128; g) G. Mahmud, K. J. M. Bishop, Y. Chegel, S. K. Smoukov, B. A. Grzybowski, *J. Am. Chem. Soc.* **2008**, *130*, 2146 – 2147; h) I. Lagzi, B. Kowalczyk, B. A. Grzybowski, *J. Am. Chem. Soc.* **2010**, *132*, 56 – 60.

[16] a) R. M. A. Roque-Malherbe, *Adsorption and diffusion in nanoporous materials*, CRC, New York, **2007**, pp. 130 – 163; b) W. M. Deen, *AIChE J.* **1987**, *33*, 1409 – 1425; c) B. D. Prasher, Y. H. MA, *AIChE J.* **1977**, *23*, 303 – 311.

[17] M. Eddaoudi, J. Kim, N. Rosi, D. Vodak, J. Wachter, M. O'Keeffe, O. M. Yaghi, *Science* **2002**, *295*, 469 – 472.

[18] a) Y. Onganer, E. L. Quitens, *J. Phys. Chem.* **1992**, *96*, 7996 – 8001; b) M. Arik, Y. Onganer, *Chem. Phys. Lett.* **2003**, *375*, 126 – 133.

[19] a) H. Schönherr, M. W. J. Beulen, J. Bügler, J. Huskens, F. C. J. M. van Veggel, D. N. Reinhoudt, G. J. Vancso, *J. Am. Chem. Soc.* **2000**, *122*, 4963 – 4967; b) M. A. C. Broeren, B. F. M. de Waal, M. H. P. van Genderen, H. M. H. F. Sander, G. Fytas, E. W. Meijer, *J. Am. Chem. Soc.* **2005**, *127*, 10334 – 10343.

[20] A. Hatch, E. Garcia, P. Yager, *Proc. IEEE* **2004**, *92*, 126 – 139.

[21] J. Crank, *The Mathematics of Diffusion*, Oxford University Press, London, **1975**.

[22] Since the exact nature of PB binding sites on the MOF-5 scaffold is not known, it is assumed—based on the CPK model of PB and MOF-5—that maximally one PB molecule can fit into one MOF-5 cavity (with a volume of 2.10×10^{-27} m^3). This results in a total concentration of binding sites of 0.79 M.

[23] a) T. Cherdhirankorn, A. Best, K. Koynov, K. Peneva, K. Muellen, G. Fytas, *J. Phys. Chem. B* **2009**, *113*, 3355 – 3359; b) R. Raccis, A. Nikoubashman, M. Retsch, U. Jonas, K. Koynov, H.-J. Butt, C. N. Likos, G. Fytas, *ACS Nano* **2011**, *5*, 4607 – 4616.

[24] W. Al-Soufi, B. Reija, M. Novo, S. Felekyan, R. Kuhnemuth, C. A. M. Seidel, *J. Am. Chem. Soc.* **2005**, *127*, 8775 – 8784.

